Numerical study of the drift of scroll waves by optical feedback in cardiac tissue

Yuan-Xun Xia,[1] Ling-Hao Xie,[1] Yin-Jie He,[2] Jun-Ting Pan,[3] Alexander V. Panfilov,[4,5,6,*] and Hong Zhang[1,†]

[1]*Zhejiang Institute of Modern Physics, School of Physics, Zhejiang University, Hangzhou 310058, China*

[2]*Information Engineering College, Zhijiang College of Zhejiang University of Technology, Shaoxing 312030, China*

[3]*Ocean College, Zhejiang University, Zhoushan 316021, China*

[4]*Department of Physics and Astronomy, Ghent University, Ghent 9000, Belgium*

[5]*Laboratory of Computational Biology and Medicine, Ural Federal University, Ekaterinburg 620002, Russia*

[6]*World-Class Research Center "Digital Biodesign and Personalized Healthcare," Sechenov University, Moscow 119146, Russia*

(Received 5 July 2023; accepted 16 November 2023; published 11 December 2023)

Nonlinear waves were found in various types of physical, chemical, and biological excitable media, e.g., in heart muscle. They can form three-dimensional (3D) vortices, called scroll waves, that are of particular significance in the heart, as they underlie lethal cardiac arrhythmias. Thus controlling the behavior of scroll waves is interesting and important. Recently, the optical feedback control procedure for two-dimensional vortices, called spiral waves, was developed. It can induce directed linear drift of spiral waves in optogenetically modified cardiac tissue. However, the extension of this methodology to 3D scroll waves is nontrivial, as optogenetic signals only penetrate close to the surface of cardiac tissue. Here we present a study of this extension in a two-variable reaction-diffusion model and in a detailed model of cardiac tissue. We show that the success of the control procedure is determined by the tension of the scroll wave filament. In tissue with positive filament tension the control procedure works in all cases. However, in the case of negative filament tension for a sufficiently large medium, instabilities occur and make drift and control of scroll waves impossible. Because in normal cardiac tissue the filament tension is assumed to be positive, we conclude that the proposed optical feedback scheme can be a robust method in inducing the linear drift of scroll waves that can control their positions in cardiac tissue.

DOI: 10.1103/PhysRevE.108.064406

I. INTRODUCTION

Nonlinear waves in excitable media often organize themselves into vortexlike rotating waves known in two dimensions as spiral waves, and in three dimensions as scroll waves [1]. These rotating waves have been observed in a variety of physical, chemical, and biological systems [2]. They have been under active investigation as an interesting example of self-organization in nonlinear systems [3], and they have important practical applications in cardiology as well [4–6]. The interest in the dynamics of scroll waves has significantly broadened in the past decades as such self-sustained rotating wave activities are thought to be responsible for certain types of cardiac arrhythmias, such as ventricular tachycardia and fibrillation, the main causes of sudden cardiac death [7–10].

A scroll wave can be viewed as a vortex obtained by the spatial shifting of a two-dimensional (2D) rotating spiral wave transversally to its rotation plane [2,11,12]. Similar to a spiral wave rotating around a point of phase singularity (PS), a scroll wave rotates around a curve called a filament, which connects the singularity points of the corresponding spiral waves. The global behavior of a scroll wave is quite complex, but some of its features can be well described by the motion of its filament [13,14]. The long-term behavior of filaments was shown to depend on the property of the filament called filament tension, which can be positive or negative [11,15,16]. Depending on the sign of the filament tension, two main dynamic phenomena have been observed: when the tension is positive (normally or highly excitable media), the filament tends to decrease its length and thus small perturbations of a straight filament will tend to disappear; when the tension is negative (weakly excitable media), a straight filament in a large enough domain is unstable, as small perturbations will grow causing an initially straight scroll to decay into an unordered turbulent state [17–19].

The ventricles of the heart have thick walls and are clearly three-dimensional (3D) systems; thus vortices which occur there are scroll waves. Thus controlling the behavior of scroll waves is important and meaningful. Over the years many methods to control scroll waves have been put forward [19–30]. However, most of these methods were not related to cardiac tissue, or could not be applied to it due to technical limitations.

Recently, novel experimental methodologies in cardiac research were developed. One of them is optogenetics [31,32], where by the expression of light-sensitive ion channels, it became possible to affect the cardiac excitation by the application of light. Optogenetic stimulation has many noteworthy advantages over conventional methods, including selective electrophysiological modulation in specifically targeted cell

*Corresponding author: alexander.panfilov@ugent.be

†Corresponding author: hongzhang@zju.edu.cn

subpopulations, high-resolution spatiotemporal control via patterned illumination, and the use of different opsins to elicit inward or outward transmembrane currents [33]. Based on the optogenetic method, several interesting dynamic phenomena of spiral waves in optogenetically modified cardiac tissue were observed and some schemes to control them were modeled [34–37]. However, all of them were applied in 2D cases.

In our previous study [38], we proposed a method which allows one to induce a controlled drift of spiral waves in 2D optogenetical cardiac tissue. This method is based on the idea which was used to control the drift of spiral waves in the Belousov-Zhabotinsky (BZ) reaction [39–41], by the external electrical field. Although such an approach is impossible to apply to cardiac tissue directly, as the action of the external field on the heart does not result in the gradient terms in the equations describing wave propagation, we proposed a method that solves such a problem for optogenetical cardiac tissue. We showed that a similar action can be realized by a feedback procedure in which some properties of the excitation pattern are extracted and then can be used to modulate the light intensity applied to optogenetic cardiac tissue. Using this method we obtained linear drift of spiral waves in cardiac tissue and were able to control them by light in the same way as in the BZ reaction with an applied external electric field. Such a method can be applied to 2D systems, such as cardiac cell cultures or atria of the heart which have thin walls. However, this method cannot be claimed for the ventricles of the heart which are 3D systems. In contrast to 2D systems, the optical feedback control for scroll waves in 3D systems is more complicated and rather difficult. First, as light cannot penetrate through all the thickness of the heart, the control procedure will only affect part of the scroll waves located close to the surface of the heart. Second, it is also important to consider additional 3D effects of its own filament dynamics of the scroll wave, namely, the filament tension.

In this paper, we investigate how the control method of spiral waves considered in Ref. [38] will work for 3D cases. We use the two-variable FitzHugh-Nagumo model and the detailed Luo-Rudy model for cardiac cells to reproduce the effect of illumination of 3D optically modified cardiac tissue and study in detail the effect of the optical feedback on scroll waves with positive or negative filament tension.

II. MODELS

A. FitzHugh-Nagumo model

We use the FitzHugh-Nagumo (FHN) model, a two-component (u and v) reaction-diffusion system, to describe the excitable medium [42,43]:

$$\frac{\partial u}{\partial t} = D\nabla^2 u + f(u, v) + I_{\text{optp}}, \tag{1a}$$

$$\frac{\partial v}{\partial t} = g(u, v), \tag{1b}$$

where $f(u, v) = (u - u^3/3 - v)/\varepsilon$ and $g(u, v) = \varepsilon(u + \beta - \gamma v)$ are the FHN kinetics; u and v are the fast (potential) and the slow (gating) variables, respectively; $D = 1$ is the diffusion coefficient of u. In this paper, the model parameters are set to be $\varepsilon = 0.22$ and $\gamma = 0.8$ for all FHN media, while $\beta = 0.58$ and $\beta = 0.78$ are used to generate scroll waves with positive filament tension in highly excitable media and with negative filament tension in weakly excitable media, respectively. The initial conditions for standard straight scroll waves (vertical filament without twists) in 3D media are obtained by first generating rotating spiral waves in 2D media and then stacking them on the top of one another along the vertical axis.

The filament tension determines the motion of the filament in the direction of its normal in Frenet coordinates and the variation of the length of the filament [16,44]. The equations for the normal velocity V_{N} and the filament tension b_2 are given by

$$V_{\text{N}} = b_2\kappa, \tag{2a}$$

$$b_2 = \text{Re}(\langle \mathbf{W}^{(1)}, \mathbf{DV}^{(1)} \rangle), \tag{2b}$$

where κ is the filament curvature, $\mathbf{V}^{(1)}$ is a Goldstone mode of the spiral wave in 2D media, $\mathbf{W}^{(1)}$ is the response function corresponding to $\mathbf{V}^{(1)}$, $\mathbf{D}$ is a diffusion matrix, and the inner product $\langle \mathbf{w}, \mathbf{v} \rangle$ stands for the scalar product in functional space. More information about the response function theory can be found in Refs. [45–47]. We compute Eq. (2b) by using the open source software "DXSPIRAL" [48]. The result is $b_2 = 0.86 > 0$ when $\beta = 0.58$ and $b_2 = -1.09 < 0$ when $\beta = 0.78$, showing that the filament tension is positive in a highly excitable medium and is negative in a weakly excitable medium, respectively.

In simulations, Eq. (1) is integrated via the Euler method with no-flux boundary conditions on all boundaries of the medium. The space step and the time step in dimensionless space and time units are $\Delta x = \Delta y = \Delta z = 0.25$ and $\Delta t = 0.005$, respectively. Simulations of the FHN model were performed in a uniform Cartesian grid in cuboid domains of varying thickness L_Z, while most of the simulations were performed in a box of size $25 \times 25 \times 12.5$. The wavelength of a spiral wave with positive filament tension is about 80 grid points. If we scale the size of the medium by wavelength λ, the size 100×100 grid points will have the size of $1.25\lambda \times 1.25\lambda$. In the case of a spiral wave with negative filament tension in which the wavelength is about 150 grid points, the size 100×100 grid points will have the size of $0.67\lambda \times 0.67\lambda$. As for the spiral period, the typical period T of a spiral wave in the FHN model is about $T = 11.0$ for positive and about $T = 23.3$ for negative filament tension, respectively.

I_{optp} is the optogenetic current in cardiac tissue which can be depolarizing or hyperpolarizing depending on which opsin is expressed [34,35,49,50]. In Eq. (1), we denote the upper and the lower roots of $f(u, v_{\text{rest}}) = 0$ as $u = u_{\text{max}}$ and as $u = u_{\text{min}}$, which correspond to the depolarizing state and the resting (hyperpolarizing) state, respectively, where v_{rest} is the value of v in the resting state. Thus we use $u = u_{\text{max}}$ and $u = u_{\text{min}}$ as a Nernst potential for the depolarizing and the hyperpolarizing current, correspondingly. Also we assume that the conductance of the optogenetic channels is g which depends on the local light intensity at given position $\vec{r} = (x, y, z)$ and time t, and that we can control the value of g locally by light. Thus we obtain for the optogenetic current the following

representations:

$$I_{\text{optp}}(x,y,z,t) = \begin{cases} I_{\text{depolarizing}} = -g(x,y,z,t)[u(x,y,z,t) - u_{\max}] \\ \text{or} \\ I_{\text{hyperpolarizing}} = -g(x,y,z,t)[u(x,y,z,t) - u_{\min}] \end{cases}. \tag{3}$$

Note that the conductance is always positive, so $g \geqslant 0$; for $u_{\min} < u < u_{\max}$, the depolarizing and the hyperpolarizing currents in Eq. (3) are positive (inward) and negative (outward), respectively.

B. Luo-Rudy model

To extend the applicability of our method to more realistic systems, we also implemented the widely used Luo-Rudy model for membrane action potentials [51]:

$$\frac{\partial V}{\partial t} = -\frac{I_{\text{ion}} + I_{\text{optp}}}{C_m} + D\nabla^2 V, \tag{4a}$$

$$I_{\text{ion}} = I_{\text{Na}} + I_{\text{si}} + I_K + I_{K1} + I_{Kp} + I_b, \tag{4b}$$

where V is the transmembrane potential, $C_m = 1\,\mu\text{F/cm}^2$ is the membrane capacitance, and $D = 0.001\,\text{cm}^2/\text{ms}$ is the diffusion coefficient. I_{ion} is the total ionic current density, which contains six ionic currents: $I_{\text{Na}} = \bar{G}_{\text{Na}} m^3 h j (V - E_{\text{Na}})$ is the fast sodium current; $I_{\text{si}} = \bar{G}_{\text{si}} df (V - E_{\text{si}})$ is the slow inward current; $I_K = \bar{G}_K x x_1 (V - E_K)$ is the time-dependent potassium current; $I_{K1} = \bar{G}_{K1} K1_\infty (V - E_{K1})$ is the time-independent potassium current; $I_{Kp} = 0.0183 K_p (V - E_{Kp})$ is the plateau potassium current; and $I_b = 0.039\,21(V + 59.87)$ is the time-independent background current. m, h, j, d, f, and x are gating variables, which are described by $dy/dt = (y_\infty - y)/\tau_y$, where y represents the gating variables. $\bar{G}_{\text{Na}}$, $\bar{G}_{\text{si}}$, $\bar{G}_K$, and $\bar{G}_{K1}$ are the maximum conductance of I_{Na}, I_{si}, I_K, and I_{K1}, respectively. For more details of the Luo-Rudy model, see Ref. [51]. We consider the case of a scroll wave with positive or negative filament tension, the details of which can be found in the parameter region of the Luo-Rudy model in Ref. [52]. For the positive case, we set $\bar{G}_{\text{Na}} = 3.70\,\text{mS/cm}^2$, $\bar{G}_{\text{si}} = 0.00\,\text{mS/cm}^2$, $\bar{G}_K = 0.423\,\text{mS/cm}^2$, $j \equiv 1$, and for the negative case we set $\bar{G}_{\text{Na}} = 3.35\,\text{mS/cm}^2$, $\bar{G}_{\text{si}} = 0.00\,\text{mS/cm}^2$, $\bar{G}_K = 0.423\,\text{mS/cm}^2$, $j \equiv 1$. In simulations, the space and the time steps are $\Delta x = \Delta y = \Delta z = 0.02\text{cm}$ and $\Delta t = 0.01\text{ms}$, respectively. Simulations of the Luo-Rudy model were performed in a uniform Cartesian grid in cuboid domains of various sizes with no-flux boundary conditions. The wavelength of a spiral wave with positive filament tension is about 75 grid points. Scaling the size of the medium by wavelength λ, the size 100×100 grid points will have the size of $1.33\lambda \times 1.33\lambda$. In the case of a spiral wave with negative filament tension, the wavelength is about 130 grid points, and grid points of size 100×100 would have a size of $0.77\lambda \times 0.77\lambda$. The typical period T of a spiral wave is about $T = 56\,\text{ms}$ for positive and about $T = 95\,\text{ms}$ for negative filament tension, respectively.

To model the optogenetic current in cardiology, we use a four-state Markov light-sensitive Channelrhodopsin-2 (ChR2) model to describe the depolarizing current I_{optp} in Eq. (4a) [53,54], which is based on the experimental measurements of this current [55]. The equation for the ChR2 model is as follows:

$$I_{\text{optp}} = g_{\text{ChR2}} G(V)(O_1 + \gamma O_2)(V - E_{\text{ChR2}}), \tag{5}$$

with

$$G(V) = \frac{10.6408 - 14.6408\exp(-V/42.7671)}{V},$$

$$\frac{dO_1}{dt} = -(G_{d1} + e_{12})O_1 + e_{21}O_2 + k_1 C_1,$$

$$\frac{dO_2}{dt} = e_{12}O_1 - (G_{d2} + e_{21})O_2 + k_2 C_2,$$

$$\frac{dC_1}{dt} = G_{d1}O_1 - k_1 C_1 + G_r C_2,$$

$$\frac{dC_2}{dt} = G_{d2}O_2 - (k_2 + G_r)C_2,$$

$$O_1 + O_2 + C_1 + C_2 = 1,$$

where $g_{\text{ChR2}} = 0.4\,\text{mS/cm}^2$ is the maximal conductance; $G(V)$ is the voltage-dependent rectification function; O_1, O_2, C_1, and C_2 are the open and the closed state probabilities; $\gamma = 0.1$ is the conductance ratio of O_2/O_1; and $E_{\text{ChR2}} = 0\,\text{mV}$ is the reversal potential for ChR2. G_{d1}, G_{d2}, G_r, e_{12}, e_{21}, k_1, and k_2 are kinetic parameters for the four-state Markov model:

$$G_{d1} = 0.075 + 0.043\tanh\left(-\frac{V+20}{20}\right),$$

$$G_{d2} = 0.05,$$

$$G_r = 4.345\,87 \times 10^{-5} \times \exp(-0.021\,153\,927\,4V),$$

$$e_{12} = 0.011 + 0.005\ln\left(1 + \frac{I_{\text{light}}}{0.024}\right),$$

$$e_{21} = 0.008 + 0.004\ln\left(1 + \frac{I_{\text{light}}}{0.024}\right),$$

$$k_1 = 0.8535Fp, \quad k_2 = 0.14Fp,$$

$$F = \frac{0.0006 I_{\text{light}}\lambda}{w_{\text{loss}}}, \quad \frac{dp}{dt} = \frac{S_0 - p}{\tau_{\text{ChR2}}},$$

$$S_0 = 0.5\{1 + \tanh[120(100 I_{\text{light}} - 0.1)]\},$$

where I_{light} is the light intensity, $\lambda = 470\,\text{nm}$ is the wavelength of light, $w_{\text{loss}} = 0.77$ is the scaling factor for losses of photons, $\tau_{\text{ChR2}} = 1.3\,\text{ms}$ is the time constant of ChR2 activation, and F is the photon flux. p and S_0 are the state variables, denoting the time- and the light-dependent activation functions for ChR2, respectively.

C. Control scheme

First, let us consider a 2D analog of Eq. (3) with just two spatial coordinates, x and y. In a recent work [38], we showed that a special optical feedback control scheme can be used to induce the same type of directed linear drift of spiral waves in cardiac tissue as in the BZ reaction with an applied external dc electric field.

In more detail, the effect of the electric field in the BZ reaction is usually described by an additional gradient term $-\vec{E} \cdot \nabla u$ in the equation for the diffusive species [39,40,56]. Without loss of generality, we only consider that the dc electric

field $\vec{E}$ is directed parallel to the x axis (i.e., $E_x > 0,\ E_y = 0$) as the system has rotating symmetry. In this case, the effect of the dc electric field on the BZ reaction can be described by the following additional term for the reaction-diffusion equations describing the BZ reaction [we do not provide the equations for the BZ reaction here, but they are similar to Eq. 1(a) for cardiac tissue]:

$$\begin{aligned} -E_x \partial u/\partial x \geqslant 0 \ \text{ if } \quad \partial u/\partial x \leqslant 0, \\ -E_x \partial u/\partial x < 0 \ \text{ if } \quad \partial u/\partial x > 0. \end{aligned} \tag{6}$$

In Ref. [38], we showed that we can reproduce a similar term in cardiac tissue for the FHN model by activating optogenetic currents through a feedback control scheme, as described by the following equation:

$$I_{\text{optp}}(x,y,t) = \begin{cases} -g_o|\partial u(t-\tau_1)/\partial x|[u(t)-u_{\max}] & \text{if} \quad \partial u(t-\tau_1)/\partial x \leqslant 0 \\ -g_o|\partial u(t-\tau_1)/\partial x|[u(t)-u_{\min}] & \text{if} \quad \partial u(t-\tau_1)/\partial x > 0 \end{cases}, \tag{7}$$

where we assume that the optical system produces light that activates the optogenetic currents whose conductance is proportional to $|\partial u/\partial x|$ with a scaling factor g_o, and $u_{\min} < u < u_{\max}$; two types of optogenetic currents (depolarizing and hyperpolarizing) are used according to the sign of $\partial u/\partial x$; τ_1 is the operational time delay in a feedback system. We set $\tau_1 = 0.01T$ in which T is the period of spiral waves in the FHN model. Equation (7) requires simultaneous expressions in the cell of two different types of light-sensitive ion channels and the possibility to control them independently. If only one type of the ion channels is available, we have some possible realization that only relies on the depolarizing or on the hyperpolarizing current:

$$I_{\text{optp}}(x,y,t) = \begin{cases} -g_o|\partial u(t-\tau_1)/\partial x|(u(t)-u_{\max}) & \text{if} \quad \partial u(t-\tau_1)/\partial x \leqslant 0 \\ 0 & \text{if} \quad \partial u(t-\tau_1)/\partial x > 0 \end{cases}, \tag{8}$$

where only the depolarizing current is used, or

$$I_{\text{optp}}(x,y,t) = \begin{cases} 0 & \text{if} \quad \partial u(t-\tau_1)/\partial x \leqslant 0 \\ -g_o|\partial u(t-\tau_1)/\partial x|[u(t)-u_{\min}] & \text{if} \quad \partial u(t-\tau_1)/\partial x > 0 \end{cases}, \tag{9}$$

where only the hyperpolarizing current is used. For further details please see Ref. [38].

In the Luo-Rudy model, we use only the ChR2 depolarizing current. Similar to Eq. (8), the scheme of our feedback system is to control the light intensity of the ChR2 model in the following form [38]:

$$I_{\text{light}}(x,y,t) = \begin{cases} I_o|\partial V(t-\tau_1)/\partial x| & \text{if} \quad \partial V(t-\tau_1)/\partial x \leqslant 0 \\ 0 & \text{if} \quad \partial V(t-\tau_1)/\partial x > 0 \end{cases}, \tag{10}$$

where $\tau_1 = 0.01T$, in which T is the period of spiral waves in the Luo-Rudy model, and I_o is the scaling factor of the light intensity.

In this paper, we apply this scheme in the following way. As the ventricles of the heart are 3D media, our optogenetic signal will influence only the surface of the heart, and the intensity of light will decrease with the thickness of the ventricles of the heart by the exponential law due to scattering [49]. We assume that the light is applied to the top of the medium, where $z = z_0$; then the optogenetic current inside the medium will be proportional to the reduced light intensity:

$$I_{\text{optp}}(x,y,z,t) = e^{-\frac{z_0-z}{\delta}} I_{\text{optp}}(x,y,z_0,t), \tag{11}$$

where $\delta = 0.5$ is the attenuation length for light in the FHN model. The optogenetic current at the top $I_{\text{optp}}(x,y,z_0,t)$ can take one of the three forms identical to $I_{\text{optp}}(x,y,t)$ in Eqs. (7)–(9):

$$I_{\text{optp}}(x,y,z_0,t) = \begin{cases} -g_o|\partial u(z_0,t-\tau_1)/\partial x|[u(t)-u_{\max}] & \text{if} \quad \partial u(z_0,t-\tau_1)/\partial x \leqslant 0 \\ -g_o|\partial u(z_0,t-\tau_1)/\partial x|[u(t)-u_{\min}] & \text{if} \quad \partial u(z_0,t-\tau_1)/\partial x > 0 \end{cases}, \tag{12}$$

$$I_{\text{optp}}(x,y,z_0,t) = \begin{cases} -g_o|\partial u(z_0,t-\tau_1)/\partial x|[u(t)-u_{\max}] & \text{if} \quad \partial u(z_0,t-\tau_1)/\partial x \leqslant 0 \\ 0 & \text{if} \quad \partial u(z_0,t-\tau_1)/\partial x > 0 \end{cases}, \tag{13}$$

$$I_{\text{optp}}(x,y,z_0,t) = \begin{cases} 0 & \text{if} \quad \partial u(z_0,t-\tau_1)/\partial x \leqslant 0 \\ -g_o|\partial u(z_0,t-\tau_1)/\partial x|[u(t)-u_{\min}] & \text{if} \quad \partial u(z_0,t-\tau_1)/\partial x > 0 \end{cases}. \tag{14}$$

In the Luo-Rudy model, the light intensity decreases along the z axis:

$$I_{\text{light}}(x,y,z,t) = e^{-\frac{z_0-z}{\delta}} I_{\text{light}}(x,y,z_0,t), \tag{15}$$

where $\delta = 0.057$ cm is the attenuation length measured from an irregular geometry of the rabbit ventricles with blue light illumination in Refs. [49,57]. The light intensity $I_{\text{light}}(x, y, z_0, t)$ on the top surface takes a form identical to $I_{\text{light}}(x, y, t)$ in Eq. (10):

$$I_{\text{light}}(x, y, z_0, t) = \begin{cases} I_o|\partial V(z_0, t-\tau_1)/\partial x| & \text{if } \partial V(z_0, t-\tau_1)/\partial x \leqslant 0 \\ 0 & \text{if } \partial V(z_0, t-\tau_1)/\partial x > 0 \end{cases}. \tag{16}$$

Equations (11)–(16) are the entire feedback control schemes for 3D cardiac models.

D. Filament identification

In this paper, we modify the recently developed topological charge-density-vector method to identify the filaments of the scroll waves [14]. In numerical simulation, the phase ϕ is calculated by $\phi(x, y, z, t) = \arctan 2[V(x, y, z, t+\tau_2) - V^*, V(x, y, z, t) - V^*]$ [58]. τ_2 is the time delay which is set as $0.05T$ in the Luo-Rudy model ($0.1T$ in the FHN model); constant V^* is set as -35 mV in the Luo-Rudy model (0 in the FHN model). The PS is tracked once the filament crosses one of the local sections, and the center of that plane section is considered as the PS, which is denoted by a red star in Fig. 1(a). The filament of a scroll wave is determined by connecting all the found PS points to each other at given moment of time, and the length of the resulting line is calculated as the length of the filament. The filament identified by this method is still not smooth enough due to the discretization. Additional operations were used to obtain a smoother filament in Ref. [14]. Here, we enhance the precision by employing the bilinear interpolation of the transmembrane potential V across the local cross section. Based on the PS identified through the topological charge-density-vector method as shown in Fig. 1(a), we interpolate that specific section of the medium into a 100×100 grid, compute the phase at each grid point, and subsequently apply the topological charge-density-vector method again to obtain more precise determination of the PS [Fig. 1(b)]. This interpolation procedure enables us to have smooth filaments.

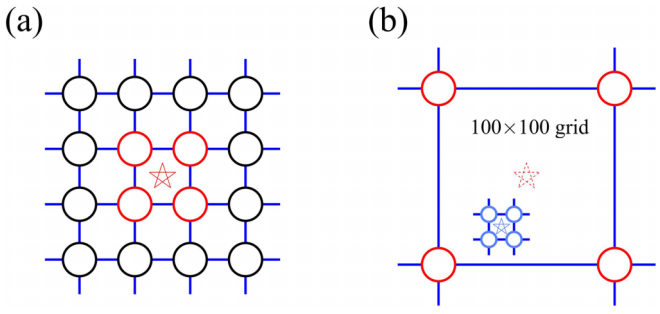

FIG. 1. Schematic representations of the modified topological charge-density-vector method. (a) The center of the local cross section (enclosed by four red grid points) is considered as a PS candidate, which is denoted by the red star. (b) The four points in (a) are interpolated into a 100×100 grid, and the PS is identified again by the same method. The blue star denotes the PS with high precision.

III. RESULTS

A. Positive filament tension

We investigate the application of the optical feedback control procedure, described by Eqs. (11) and (12), to a scroll wave with positive filament tension in the FHN model in a 3D medium. The simulation is performed in a box of size $25 \times 25 \times 12.5$, where the thickness significantly exceeds the attenuation length of light, i.e., $L_Z \gg \delta$. The filament of the rigidly rotating scroll wave is initially orthogonal to the surfaces [Fig. 2(a)]. Because we illuminate only the top surface of the medium, the optical control signal influences only scroll waves located close to the surface. However, we observe that the whole scroll wave undergoes directional drift [Fig. 2(b)]. Figures 2(c) and 2(d) show the PS trajectories of spiral waves at the top and the bottom of the medium. We see at both the top and the bottom sections the spiral waves drift along a straight line. While the directed linear drift of the spiral wave at the top of the medium is induced by the optical feedback, the drift of the spiral wave at the bottom of the medium, where there are almost no optical signals, is induced by the positive filament tension. Indeed, the induced drift at the top elongates the filament; however, the positive filament tension tries to

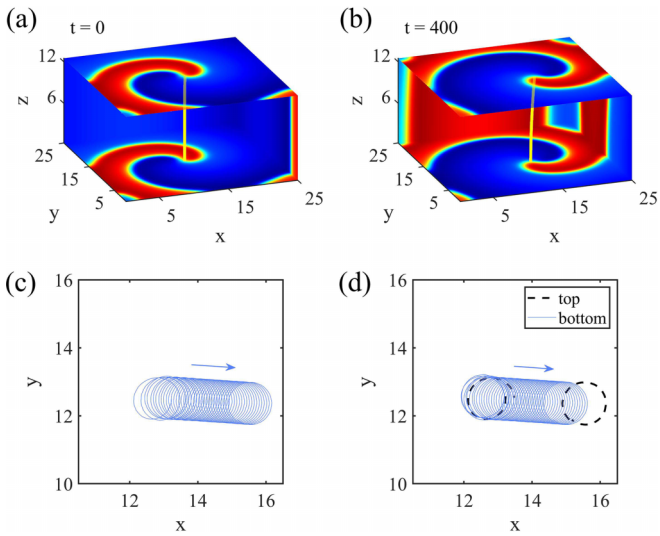

FIG. 2. The directional drift of a scroll wave under optical feedback control given by Eqs. (11) and (12), where the optogenetic signal is applied to the top of the medium. The filament tension is positive, $L_Z = 12.5$, and $g_o = 0.1$. (a) The pattern of the initial scroll wave and its filament (yellow line). (b) The pattern of the scroll wave at the end of the simulation time, $t = 400$. (c) The PS trajectory of the top spiral wave from $t = 0$ to 400. (d) The PS trajectory of the bottom spiral wave from $t = 0$ to 400. The dashed lines indicate the PS trajectories of the top spiral wave for the first and the last periods.

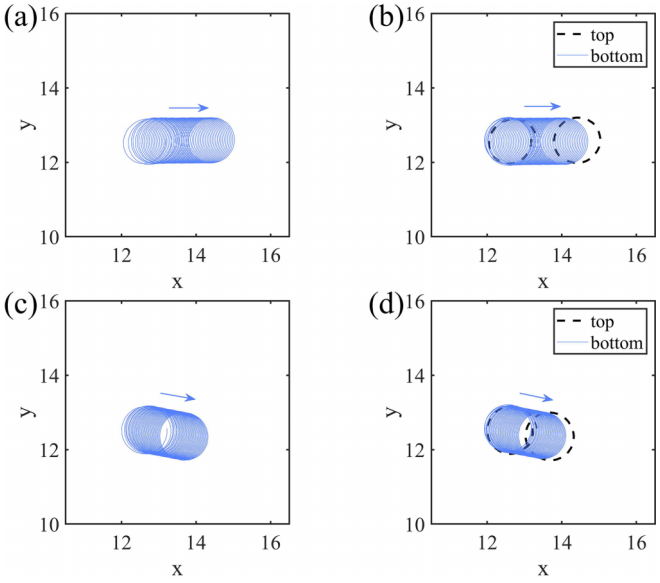

FIG. 3. The drift of scroll waves under the depolarizing or hyperpolarizing optical feedback. We show PS trajectories of the spiral waves on the top and the bottom surfaces from $t = 0$ to 400. The filament tension is positive, $L_Z = 12.5$, and $g_o = 0.1$. (a,b) Application of the depolarizing current given by Eq. (13). (c,d) Application of the hyperpolarizing current given by Eq. (14). (a,c) The PS trajectories of the top spiral wave. (b,d) The PS trajectories of the bottom spiral wave. Dashed lines show the trajectories of the first and the last rotations in (a,c).

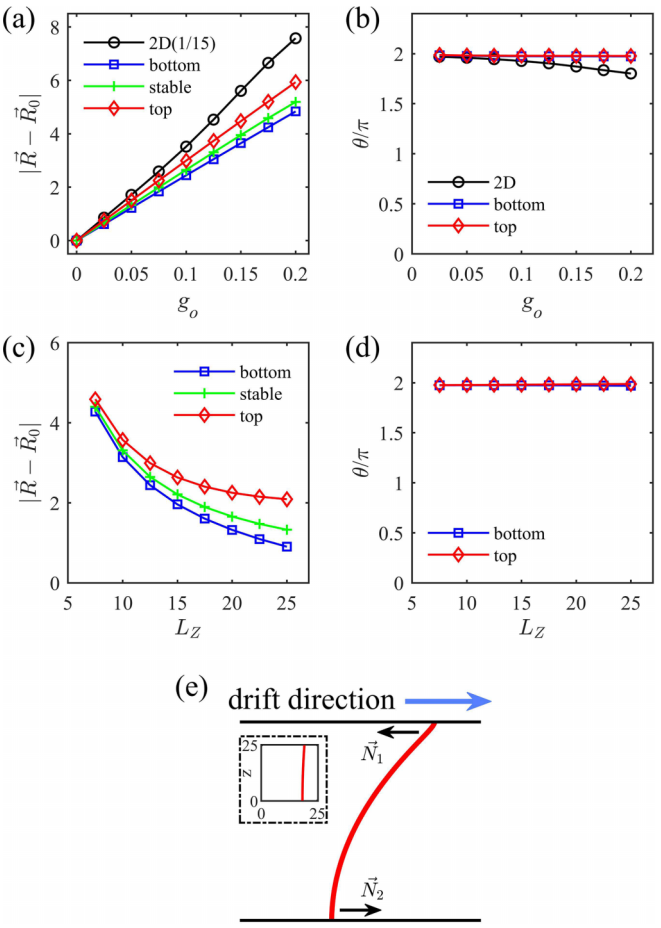

FIG. 4. The displacements of rotating centers $\vec{R} - \vec{R}_0$ for different g_o or L_Z. $\vec{R}$ is the rotating center at $t = 400$. $\vec{R}_0$ is the rotating center at $t = 0$. Red diamonds denote the displacement at the top of the media, and blue squares denote that at the bottom. Green pluses denote the displacement after the filament becomes stable. Black circles denote the displacement in the 2D system, the magnitude of which is reduced by 15 times. (a,c) Comparisons of the magnitude of displacements. (b,d) Comparisons of the direction of displacements. (a,b) Relationships between the displacement and the light intensity g_o. Parameters: $L_Z = 12.5$ and $g_o = (0{-}0.2)$. When the displacement is 0 ($g_o = 0$), the angle cannot be defined. (c,d) Relationships between the displacement and the thickness L_Z. Parameters: $g_o = 0.1$ and $L_Z = (7.5{-}25)$. The optical feedback is given by Eqs. (11) and (12). (e) The filament is bent during the light-induced drift. $\vec{N}_1$ is the normal vector to the filament at the top. $\vec{N}_2$ is the normal vector to the filament at the bottom. This filament shape is from (c) where $L_Z = 25$. The horizontal coordinate is magnified by 15 times. The inset shows the original filament without magnification in the drift plane in a $25 \times 25 \times 25$ box.

decrease the filament length, which results in similar drift at the bottom of the medium. It can be observed that the drift of the spiral wave at the bottom lags a little bit behind that at the top as shown in Fig. 2(d). This indicates some delay in the shortening process and confirms that the drift is induced from the top surface.

In Fig. 3, we study some alternative implementation in the same $25 \times 25 \times 12.5$ box: Eqs. (11) and (13), using only the depolarizing current [Figs. 3(a) and 3(b)], or Eqs. (11) and (14), applying only the hyperpolarizing current [Figs. 3(c) and 3(d)]. It is noted that both the top and the bottom spiral waves undergo directional drift, which is consistent with Fig. 2 where both currents are present. However, the drift observed in Fig. 3 occurs at slower speeds and with slightly different drift angles.

During directional drift, the filament curves, which can be demonstrated by comparing the displacement of the rotating centers of the top and the bottom spiral waves. As shown in Fig. 2, we observed that the bottom spiral waves consistently lagged behind the top spiral waves in their drift. In Fig. 4, we measure the displacement of the rotating center $\vec{R} - \vec{R}_0$, where $\vec{R}_0$ is the rotating center at $t = 0$ and $\vec{R}$ is the rotating center at $t = 400$. $\vec{R}(t)$ is calculated by averaging the position of the PS during the full rotation periods. The angle between the vector $\vec{R} - \vec{R}_0$ and the x axis is θ. Three-dimensional simulations are performed in boxes varying from $25 \times 25 \times 7.5$ to $25 \times 25 \times 25$. Two-dimensional simulations are performed in a 150×100 square domain.

In the absence of light illumination ($g_o = 0$), the filament remains straight and has no drift [see Fig. 4(a)]. By increasing g_o, we see that the displacement increases with increasing g_o; however, it is always substantially less than that in 2D tissue [note that in Fig. 4(a), we scale the 2D displacement by $1/15$]. We also see that the difference in the rotating center displacement between the top and the bottom spiral waves increases with increasing g_o. In Fig. 4(c), we observed that increasing

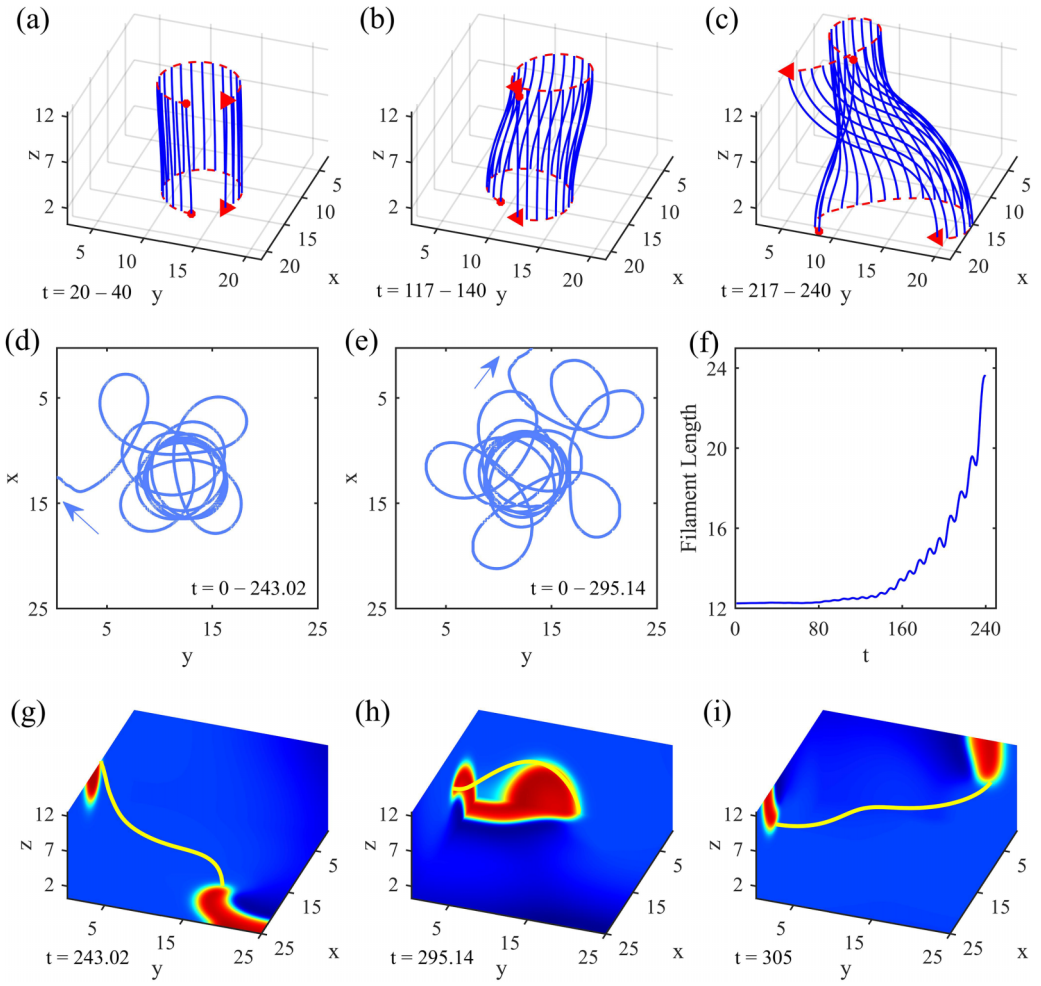

FIG. 5. Evolution of a scroll wave with negative filament tension under optical feedback; $L_Z = 12.5$ and $g_o = 0.06$. (a–c) Evolution of the filament shown in blue solid lines. The red dashed lines denote the PS trajectories at the top and the bottom, with red dots and triangles being the starting and the ending points, respectively. (a) Evolution from $t = 20$ to 40, when the filament is still straight. (b) $t = 117-140$. The filament curves. (c) $t = 217-240$. The filament expands with complex motion. (d) $t = 0$ to 243.02. The PS trajectory of the top spiral wave is close to a circle at the beginning and expands in the shape of petals until the PS collides with the boundary. (e) $t = 0$ to 295.14. The PS trajectory of the bottom spiral wave expands in the shape of petals until the PS collides with the boundary. (f) The filament length increases with time. (g–i) The pattern of the scroll wave and its filament (yellow line) at different times. (g) $t = 243.02$. The filament shape and the scroll wave pattern when the top PS collides with the boundary. (h) $t = 295.14$. The filament shape and scroll wave pattern when the bottom PS collides with the boundary. (i) $t = 305$. The filament becomes horizontal and spirals move to the sides of the medium after both the top and the bottom PSs collide with the boundary.

of L_Z results in a reduced displacement, but an increased difference in the rotating center displacement between the top and the bottom spiral waves. We remove the light source after $t = 400$. Because in the positive filament tension case, the filament tries to decrease its length, the curved filament will turn back to a stable straight filament. We then measure the displacement of its center of rotation and define it as the displacement after the filament becomes stable [green lines in Figs. 4(a) and 4(c)].

In Figs. 4(b) and 4(d), we show that altering either g_o or L_Z has no impact on the drift angle of the scroll wave under the optical feedback. In summary, increasing g_o or decreasing L_Z can enhance the magnitude of the displacement of the rotating center while maintaining its direction. Note that in Fig. 4(b), the drift direction of the 2D spiral wave slightly changes under the large light intensity.

The displacement in 3D, which is significantly less than that in 2D tissue, is another result caused by the positive filament tension. The light-induced drift of the filament in the upper sections bends the filament. We know that due to the no-flux boundary conditions, the filament is orthogonal to the top and the bottom surfaces. This means that the total angular change along the filament should be zero. Thus, if at the top the filament is shifted due to its drift, in close proximity to that region the filament will have such curvature that the normal vector to the filament ($\vec{N}_1$) at the top will point to the direction which is opposite to the direction of the induced drift [see Fig. 4(e)]. However, at the bottom the normal vector to the

filament ($\vec{N}_2$) will point to the direction which coincides with the direction of the induced drift. As a result, we will obtain the drift at the bottom; however, the curvature-related drift will reduce its velocity at the top of the medium [see Eq. (2)]. Because of this, the displacement in 3D will be shorter than that in 2D.

B. Negative filament tension

We also investigate the application of the optical feedback control procedure to a scroll wave with negative filament tension. The simulation is performed in a box of size $25 \times 25 \times 12.5$. In this case, the thickness is also $L_Z = 12.5$. In the same way as in the highly excitable case with positive filament tension, we apply the illumination on the top surface of the medium by the optical feedback scheme [as described by Eqs. (11) and (12)]. We find that in contrast with the case of positive filament tension the feedback system does not induce any directional drift of the scroll wave even at the top. Instead, filaments with negative tension tend to elongate.

The initial condition for the scroll wave with negative filament tension is a straight scroll wave obtained by the direct stacking of identical 2D rigidly rotating spiral waves. This configuration remains stable in the absence of light or other perturbations, the same as for the positive filament tension case. In each layer we see the same rigidly rotating spiral waves and thus the filament remains straight. Evolution of the filament and PS trajectories under the optical feedback is shown in Fig. 5. As seen from Figs. 5(a)–5(c), the length of the filament gradually increases while its motion follows a complex trajectory. Figures 5(d) and 5(e) illustrate the trajectories of the top and the bottom PSs. In the excitable medium with negative filament tension, the filament exhibits complex motion instead of directional drift. Figure 5(f) displays the variation in filament length over time during complex motion. The length of the filament increases monotonically with time, except for some fluctuations. In Figs. 5(g) and 5(h), we show the scroll wave patterns and filament shapes that result from the collision of the PSs with the top and the bottom boundaries at $t = 243.02$ and $t = 295.14$, respectively. After the collision we find a horizontal filament at $t = 305$ [Fig. 5(i)].

C. Luo-Rudy model

In Figs. 2–5, we applied the optical feedback control to a simplified FHN model of cardiac tissue with a simple description of the optogenetic current. In order to investigate whether such scheme works for biophysically motivated cardiac channelrhodopsin models, we apply our feedback scheme [Eqs. (15) and (16)] to the ChR2 depolarizing current included in the biophysically accurate Luo-Rudy model for cardiac tissue.

We first study the case of a rigidly rotating scroll wave with positive filament tension. The simulation is performed in a box of size $3 \times 3 \times 1\,\mathrm{cm}^3$. The filament is initially orthogonal to the top and the bottom surfaces of the medium. Figure 6(a) shows the initial condition of the scroll wave with a straight filament, which is stable in the absence of light; i.e., $I_o = 0$. By applying the optical feedback to the top surface, we observe the directional drift of the scroll wave [Fig. 6(b)]. This result

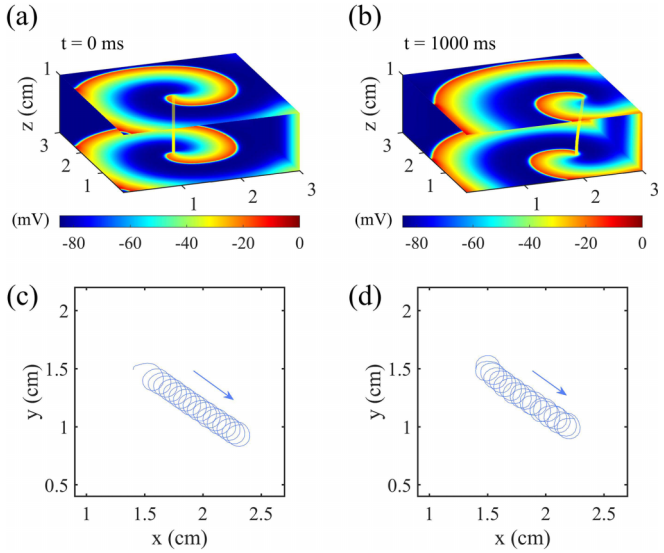

FIG. 6. The drift of a scroll wave with positive filament tension under the feedback scheme in the Luo-Rudy model; $L_Z = 1$cm, and $I_o = 50 \times 10^{-5}$. (a) The initial condition ($t = 0$ms) of the scroll wave with its vertical filament. (b) The pattern of the scroll wave at $t = 1000$ms. The scroll wave drifts toward the boundary and the filament becomes curved. (c) The PS trajectory of the spiral wave at the top. (d) The PS trajectory of the spiral wave at the bottom.

is similar to that obtained in the FHN model. We have directed linear drift of the spiral waves at both the top and the bottom of the medium [Figs. 6(c) and 6(d)].

Figure 7 demonstrates that our method does not induce the directional drift for the scroll wave with negative filament tension. The simulation is performed in a box of size $4 \times 4 \times 1\,\mathrm{cm}^3$. Due to the complex motion of the filament, we present patterns at three different time points from Fig. 7(a), the scroll wave with a straight filament which is stable in the absence of light, to Fig. 7(c), when the scroll wave filament is elongated due to its drift induced by light. In Fig. 7(d), we observe that the filament length increases over time, indicating the filament is unstable. Figures 7(e) and 7(f) show the PS trajectories of the spiral waves at the top and the bottom of the medium.

IV. DISCUSSION

In this paper we show that the optical control scheme proposed in Ref. [38] on the basis of directional drift under an external electric field in the BZ reaction can be applied in 3D cardiac tissue. However, it reliably works only for the case of positive filament tension. In the case of negative filament tension for the studied thickness of the medium 12.5 in the FHN model this method fails, due to the instability of the negative filament tension. However, this instability can be removed if the thickness of the medium is decreased [52]. In Fig. 8, we apply the feedback control to the FHN model with different thicknesses L_Z, keeping the other parameters the same as in Fig. 5. Figures 8(e) and 8(f) display the same result as in Fig. 5 (where $L_Z = 12.5$), but with trajectories plotted from $t = 0$ to 200 for easier comparisons. When $L_Z = 8.5$, the thickness is still much larger than the attenuation length $\delta = 0.5$;

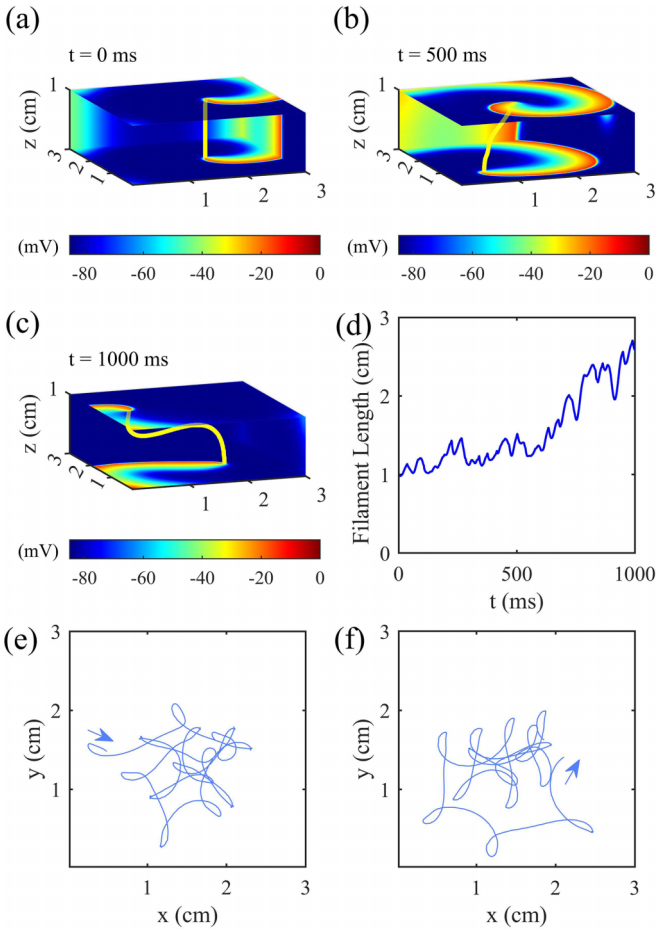

FIG. 7. Evolution of a scroll wave with negative filament tension in the Luo-Rudy model; $L_Z = 1$cm and $I_o = 50 \times 10^{-5}$. (a–c) The pattern of the scroll wave and its filament at $t = 0,\ 500,\ 1000$ ms, respectively. (d) The filament length with time. (e) The PS trajectory of the top spiral wave from $t = 0$ to 1000 ms. (f) The PS trajectory of the bottom spiral wave from $t = 0$ to 1000ms.

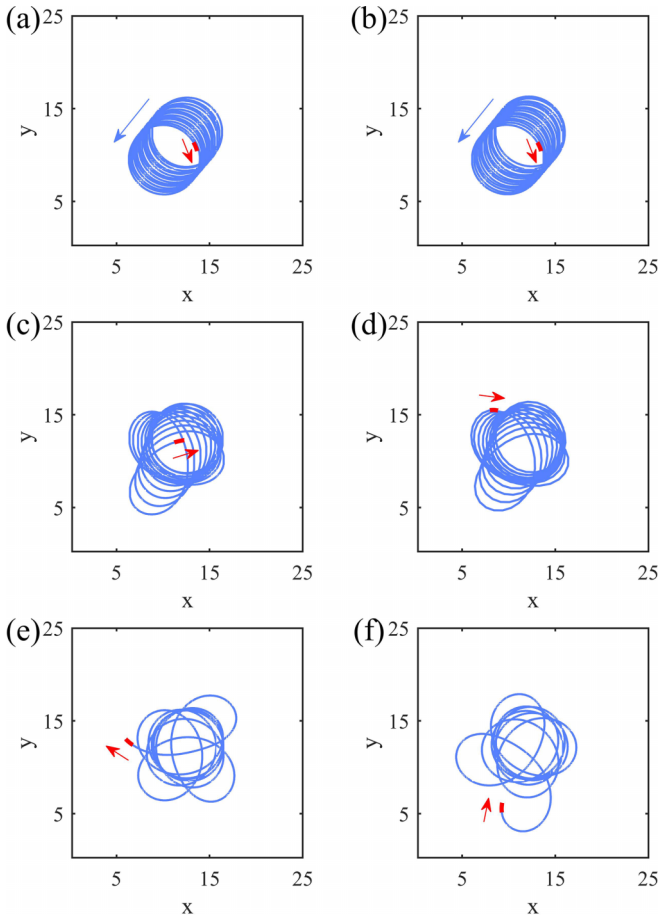

FIG. 8. The top and the bottom PS trajectories of the scroll wave with negative filament tension in the FHN model under the optical feedback control for different medium thickness. The red line denotes the trajectory at the final time point, while its direction is indicated by a red arrow. (a,b) $L_Z = 8.5$ and $t = 0-350$. The optical feedback induces directional drift of the scroll wave in 3D media. (c,d) $L_Z = 10$ and $t = 0-350$. PSs at the top and the bottom have different trajectories. (e,f) $L_Z = 12.5$ and $t = 0-200$. The result is similar to that in Figs. 5(d) and 5(e). (a,c,e) The PS trajectories at the top of the medium. (b,d,f) The PS trajectories at the bottom of the medium.

both the spiral waves on the top and the bottom surfaces drift along a straight line [Figs. 8(a) and 8(b)]. Figures 8(c) and 8(d) (where $L_Z = 10$) show similar results as in Figs. 8(e) and 8(f) (where $L_Z = 12.5$). Namely, under the feedback control, the PSs of the top spiral wave and the bottom spiral wave have different trajectories. This means these scroll waves no longer have vertical filaments. Because in our model the wavelength of a spiral wave for the case of negative filament tension is 150 grid points, or 37.5 (because the space step in the FHN model is 0.25, the wavelength in dimensionless units is 37.5), the thickness of 8.5 corresponds to 0.227λ or about 9.1−13.6 mm if we assume that the transmural wavelength of a spiral wave in the heart is 40−60 mm [59]. Thus, for the normal human heart (the median left ventricle thickness of 9 mm [60]) we can expect that we can control scroll waves using the proposed optical scheme even in the presence of negative filament tension. Also, it is widely assumed that in normal conditions the heart has high excitability and thus positive filament tension [52]. Thus, we can assume that in most cases the proposed method can control the scroll wave drift in cardiac tissue.

In this paper, we consider the possible realization of optical feedback control. While most of the results in the FHN model have been shown in the presence of both depolarizing and hyperpolarizing photosensitive currents, experimentally it is a challenging task to express both currents simultaneously in real cells and to control them independently. Since most of the current experiments were performed for a depolarizing current, in the Luo-Rudy model we included the experiment-based model for the depolarizing current and show that our method also induces the directional drift of the scroll wave with positive filament tension.

To evaluate if the light intensity produced by our optical feedback system is realistic, we performed additional estimates. The light intensity I_{light} applied to the top surface is given by the product of I_o and $|\partial V/\partial x|$, and thus it is different at different points of the medium. Let us estimate the maximal light intensity for four examples of the directional drift of scroll waves in the Luo-Rudy model shown in Fig. 9. Simulations are performed in a box of size $3 \times 3 \times 1\,\text{cm}^3$.

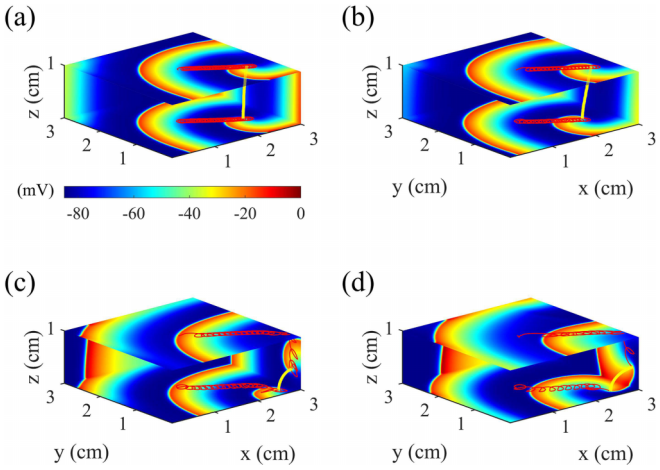

FIG. 9. Directional drift of a scroll wave with positive filament tension observed for different light intensities in the Luo-Rudy model, $L_Z = 1$ cm. The red lines denote the PS trajectories on the surface. (a) $I_o = 20 \times 10^{-5}$ and $(I_{\text{light}})_{\max} = 0.24\,\text{mW/mm}^2$. (b) $I_o = 80 \times 10^{-5}$ and $(I_{\text{light}})_{\max} = 0.96\,\text{mW/mm}^2$. (c) $I_o = 160 \times 10^{-5}$ and $(I_{\text{light}})_{\max} = 1.92\,\text{mW/mm}^2$. (d) $I_o = 320 \times 10^{-5}$ and $(I_{\text{light}})_{\max} = 3.84\,\text{mW/mm}^2$. (c,d) PSs on the top surface collide with the boundary and move to the sides of the medium. As positive tension filaments tend to decrease in length, these scroll waves become unstable and eventually disappear.

The maximum $|\partial V/\partial x|$ in Fig. 9 is about 1.2×10^3mV/cm. By taking $|\partial V/\partial x|_{\max} = 1.2 \times 10^3$ mV/cm, we can estimate the maximum intensity $(I_{\text{light}})_{\max} = I_o|\partial V/\partial x|_{\max}$ for different I_o as shown in Fig. 9. The maximum light intensity in Fig. 9 is about $3.84\,\text{mW/mm}^2$, lower than the maximum intensity $5.5\,\text{mW/mm}^2$ of experimental studies used to construct the ChR2 model [55].

Although the main aim of our paper is to study the directional drift of scroll waves and thus the control of the scroll wave position, this method can easily be used to eliminate a scroll wave from the heart. Indeed if we move a scroll wave to the boundary of the medium it will disappear. Note that in 3D the internal drift of the filament can also help to eliminate it. This is illustrated in Figs. 9(c) and 9(d). Here, after we remove the spiral wave from the top of the medium, the filament shape turns into a quarter of a ring. The scroll ring finally vanishes due to its positive filament tension.

V. CONCLUSION

In summary, we show that scroll waves with positive filament tension undergo directional drift if we apply the optical feedback control scheme and illuminate only the surface of the medium. The optical feedback control is similar to the applied external electric field in the BZ reaction and thus is a robust way to induce the desired drift of scroll waves in cardiac tissue. The optical feedback control scheme does not work for scroll waves with negative filament tension, if the thickness of the medium is sufficiently large. The filament with negative tension in relatively large systems tends to increase its length and thus the optically induced drift on the illuminated surface does not induce the drift of the filament as a whole. Because in normal conditions in cardiac tissue the filament tension is assumed to be positive, our optical feedback control scheme should be a robust way to induce the linear drift of scroll waves in cardiac tissue, which can be applied for the control of excitation processes in the heart during arrhythmias.

All computer source codes used in this study are available from the corresponding authors upon request.

ACKNOWLEDGMENTS

This work was supported by the National Natural Science Foundation of China under Grant No. 12075203, and research at Sechenov University was financed by the Ministry of Science and Higher Education of the Russian Federation within the framework of state support for the creation and development of World-Class Research Centers "Digital Biodesign and Personalized Healthcare," Grant No. 075-15-2022-304.

[1] A. T. Winfree, *The Geometry of Biological Time* (Springer, New York, 2001).
[2] A. T. Winfree and S. H. Strogatz, Nature (London) **311**, 611 (1984).
[3] J. P. Keener and J. J. Tyson, SIAM Rev. **34**, 1 (1992).
[4] J. M. Davidenko, A. V. Pertsov, R. Salomonsz, W. Baxter, and J. Jalife, Nature (London) **355**, 349 (1992).
[5] Z. Qu, G. Hu, A. Garfinkel, and J. N. Weiss, Phys. Rep. **543**, 61 (2014).
[6] S. Alonso, M. Bär, and B. Echebarria, Rep. Prog. Phys. **79**, 096601 (2016).
[7] A. T. Winfree, Science **266**, 1003 (1994).
[8] R. A. Gray, J. Jalife, A. V. Panfilov, W. T. Baxter, C. Cabo, J. M. Davidenko, and A. M. Pertsov, Science **270**, 1222 (1995).
[9] D. E. Krummen, J. Hayase, D. J. Morris, J. Ho, M. R. Smetak, P. Clopton, W.-J. Rappel, and S. M. Narayan, J. Am. Coll. Cardiol. **63**, 2712 (2014).
[10] J. Christoph, M. Chebbok, C. Richter, J. Schröder-Schetelig, P. Bittihn, S. Stein, I. Uzelac, F. H. Fenton, G. Hasenfuß, R. F. Gilmour, and S. Luther, Nature (London) **555**, 667 (2018).
[11] A. V. Panfilov and A. N. Rudenko, Phys. D (Amsterdam) **28**, 215 (1987).
[12] J. P. Keener, Phys. D (Amsterdam) **31**, 269 (1988).
[13] R. H. Clayton, E. A. Zhuchkova, and A. V. Panfilov, Prog. Biophys. Mol. Biol. **90**, 378 (2006).
[14] Y.-J. He, Y.-X. Xia, J.-T. Mei, K. Zhou, C. Jiang, J.-T. Pan, D. Zheng, B. Zheng, and H. Zhang, Phys. Rev. E **107**, 014217 (2023).
[15] A. V. Panfilov, A. N. Rudenko, and V. I. Krinsky, Biofizika **31**, 850 (1986).
[16] V. N. Biktashev, A. V. Holden, and H. Zhang, Philos. Trans. R. Soc. London Ser. A **347**, 611 (1994).
[17] H. Henry and V. Hakim, Phys. Rev. E **65**, 046235 (2002).

[18] H. Dierckx, H. Verschelde, Ö. Selsil, and V. N. Biktashev, Phys. Rev. Lett. **109**, 174102 (2012).
[19] S. Alonso, F. Sagues, and A. S. Mikhailov, Science **299**, 1722 (2003).
[20] M. Vinson, S. Mironov, S. Mulvey, and A. Pertsov, Nature (London) **386**, 477 (1997).
[21] T. Amemiya, P. Kettunen, S. Kádár, T. Yamaguchi, and K. Showalter, Chaos **8**, 872 (1998).
[22] H. Zhang, Z. Cao, N.-J. Wu, H.-P. Ying, and G. Hu, Phys. Rev. Lett. **94**, 188301 (2005).
[23] C. Luengviriya, S. C. Müller, and M. J. B. Hauser, Phys. Rev. E **77**, 015201(R) (2008).
[24] S. W. Morgan, I. V. Biktasheva, and V. N. Biktashev, Phys. Rev. E **78**, 046207 (2008).
[25] C. Qiao, Y. Wu, X. Lu, C. Wang, Q. Ouyang, and H. Wang, Chaos **18**, 026109 (2008).
[26] Z. A. Jimenez, Z. Zhang, and O. Steinbock, Phys. Rev. E **88**, 052918 (2013).
[27] J. F. Totz, H. Engel, and O. Steinbock, New J. Phys. **17**, 093043 (2015).
[28] F. Spreckelsen, D. Hornung, O. Steinbock, U. Parlitz, and S. Luther, Phys. Rev. E **92**, 042920 (2015).
[29] D.-B. Pan, Q.-H. Li, and H. Zhang, Chaos **28**, 063107 (2018).
[30] S. F. Pravdin, T. I. Epanchintsev, H. Dierckx, and A. V. Panfilov, Phys. Rev. E **104**, 034408 (2021).
[31] T. Bruegmann, D. Malan, M. Hesse, T. Beiert, C. J. Fuegemann, B. K. Fleischmann, and P. Sasse, Nat. Methods **7**, 897 (2010).
[32] A. B. Arrenberg, D. Y. R. Stainier, H. Baier, and J. Huisken, Science **330**, 971 (2010).
[33] P. M. Bolye, T. V. Karathanos, and N. A. Trayanova, JACC Clin. Electrophysiol **4**, 155 (2018).
[34] R. A. B. Burton, A. Klimas, C. M. Ambrosi, J. Tomek, A. Corbett, E. Entcheva, and G. Bub, Nat. Photonics **9**, 813 (2015).
[35] R. Majumder, I. Feola, A. S. Teplenin, A. A. De Vries, A. V. Panfilov, and D. A. Pijnappels, eLife **7**, e41076 (2018).
[36] S. Hussaini, V. Venkatesan, V. Biasci, J. M. R. Sepúlveda, R. A. Q. Uribe, L. Sacconi, G. Bub, C. Richter, V. Krinski, U. Parlitz, R. Majumder, and S. Luther, eLife **10**, e59954 (2021).
[37] R. Majumder, V. S. Zykov, and E. Bodenschatz, Phys. Rev. Appl. **17**, 064033 (2022).
[38] Y.-X. Xia, X.-P. Zhi, T.-C. Li, J.-T. Pan, A. V. Panfilov, and H. Zhang, Phys. Rev. E **106**, 024405(2022).
[39] O. Steinbock, J. Schütze, and S. C. Müller, Phys. Rev. Lett. **68**, 248 (1992).
[40] K. I. Agladze and P. De Kepper, J. Phys. Chem. **96**, 5239 (1992).
[41] A. Belmonte and J.-M. Flesselles, Europhys. Lett. **32**, 267 (1995).
[42] R. FitzHugh, Biophys. J. **1**, 445 (1961).
[43] J. Nagumo, S. Arimoto, and S. Yoshizawa, Proc. IRE **50**, 2061 (1962).
[44] A. J. Foulkes, D. Barkley, V. N. Biktashev, and I. V. Biktasheva, Chaos **20**, 043136 (2010).
[45] V. Biktashev and A. Holden, Chaos Solitons Fractals **5**, 575 (1995).
[46] I. V. Biktasheva, D. Barkley, V. N. Biktashev, G. V. Bordyugov, and A. J. Foulkes, Phys. Rev. E **79**, 056702 (2009).
[47] I. V. Biktasheva, D. Barkley, V. N. Biktashev, and A. J. Foulkes, Phys. Rev. E **81**, 066202 (2010).
[48] D. Barkley, V. N. Biktashev, I. V. Biktasheva, G. Bordyugov, and A. Foulkes, DXSPIRAL: A code for studying spiral waves on a disk; http://cgi.csc.liv.ac.uk/~ivb/SOFTware/DXSpiral.html (2010).
[49] P. M. Boyle, J. C. Williams, C. M. Ambrosi, E. Entcheva, and N. A. Trayanova, Nat. Commun. **4**, 2370 (2013).
[50] M. Funken, D. Malan, P. Sasse, and T. Bruegmann, Front. Physiol. **10**, 498 (2019).
[51] C. H. Luo and Y. Rudy, Circ. Res. **68**, 1501 (1991).
[52] S. Alonso and A. V. Panfilov, Chaos **17**, 015102 (2007).
[53] P. Hegemann, S. Ehlenbeck, and D. Gradmann, Biophys. J. **89**, 3911 (2005).
[54] K. Nikolic, N. Grossman, M. S. Grubb, J. Burrone, C. Toumazou, and P. Degenaar, Photochem. Photobiol. **85**, 400 (2009).
[55] J. C. Williams, J. Xu, Z. Lu, A. Klimas, X. Chen, C. M. Ambrosi, I. S. Cohen, and E. Entcheva, PLoS Comput. Biol. **9**, e1003220 (2013).
[56] V. Hakim and A. Karma, Phys. Rev. E **60**, 5073 (1999).
[57] M. J. Bishop, B. Rodriguez, J. Eason, J. P. Whiteley, N. Trayanova, and D. J. Gavaghan, Biophys. J. **90**, 2938 (2006).
[58] R. A. Gray, A. M. Pertsov, and J. Jalife, Nature (London) **392**, 75 (1998).
[59] K. K. Aras, N. R. Faye, B. Cathey, and I. R. Efimov, Circ.: Arrhythmia Electrophysiol. **11**, e006692 (2018).
[60] P. Stolzmann, H. Scheffel, P. T. Trindade, A. R. Plass, L. Husmann, S. Leschka, M. Genoni, B. Marincek, P. A. Kaufmann, and H. Alkadhi, Invest. Radiol. **43**, 284 (2008).